Liquid Crystal Formation in Supercoiled DNA Solutions

Svetlana S. Zakharova, Wim Jesse, Claude Backendorf, and Johan R. C. van der Maarel
Leiden Institute of Chemistry, Leiden University, 2300 RA Leiden, The Netherlands

ABSTRACT The critical concentrations pertaining to the liquid crystal formation of pUC18 plasmid in saline solutions were obtained from ^{31}P nuclear magnetic resonance, polarized light microscopy, and phase equilibrium experiments. The transition is strongly first order with a broad gap between the isotropic and anisotropic phase. The critical boundaries are strongly and reversibly dependent on temperature and weakly dependent on ionic strength. With polarized light microscopy on magnetically oriented samples, the liquid crystalline phase is assigned cholesteric with a pitch on the order of 4 μm. Preliminary results show that at higher concentrations a true crystal is formed. The isotropic–cholesteric transition is interpreted with lyotropic liquid crystal theory including the effects of charge, orientation entropy, and excluded volume effects. It was found that the molecular free energy associated with the topology of the superhelix is of paramount importance in controlling the width of the phase gap. The theoretical results compare favorably with the critical boundary pertaining to the disappearance of the isotropic phase, but they fail to predict the low concentration at which the anisotropic phase first appears.

INTRODUCTION

Under physiological conditions, deoxyribonucleic acid is often very tightly packed with concentrations up to 400 mg/mL and crowded by various macromolecular compounds such as proteins and polysaccharides. The molecular organization is largely unknown, but bears some resemblance to liquid crystalline DNA phases observed in vitro (Livolant and Leforestier, 1996). Model systems that can produce these phases are of great interest for understanding the mechanisms involved in vivo. Closed circular DNA usually exists in a supercoiled, plectonemic configuration, in which the DNA duplex is wound around another part of the same molecule to form a higher order helix. The plectonemic negative supercoiling, with a right-handed interwinding, is the most likely conformation present in vivo. The excess free energy associated with the supercoiling is used in many cellular mechanisms. Examples include the replication and transcription of DNA, the formation of nucleosomes and other protein complexes on DNA, and the formation of altered DNA structures such as cruciforms (Bates and Maxwell, 1993). Supercoiling is also of paramount importance in controlling the packaging of topologically constrained DNA in an ordered, liquid crystalline environment (Torbet and DiCapua, 1989; Reich et al., 1994).

In small angle neutron scattering (SANS) work on pUC18 bacterial plasmid (2686 bp) in saline solutions, we found that the superhelix takes locally a rod-like, interwound configuration (Zakharova et al., 2002). The supercoil can be modeled as a semiflexible wormlike cylinder with a plectonemic radius r and total length projected on the superhelical axis L. The length depends on the plectonemic opening angle, but is usually $\sim$0.4 times the length measured along the contour (Bloomfield et al., 2000). Electrostatic interactions among supercoils are screened over a relatively short distance on the order of the plectonemic diameter and, due to charge renormalization by counterion condensation (Manning, 1969) the effective charge is quite moderate. Accordingly, the supercoils do not interact too strongly, and intermolecular interference could be accounted for in the second virial approximation. The plectonemic opening angle was observed to be relatively constant and close to 58°, but it was necessary to include a significant variation in plectonemic radius and pitch in the description of the single-coil scattering function. Furthermore, the radius and pitch of the superhelix were seen to decrease significantly with increasing plasmid concentration prior and covering the transition to the liquid crystalline phase. Key to understanding this is that the intermolecular distance becomes on the order of the effective diameter of the supercoil, and, to accommodate the molecules in the confined state, the radius has to decrease at the cost of a significant elastic bending and twisting energy of the duplex. It is our hypothesis that the molecular free energy associated with this change in topology is of great consequence in controlling the phase transition.

The key factor for the formation of an ordered phase in a semiflexible polymer solution is the volume excluded by a particle to another particle (Onsager, 1949). The excluded volume depends on mutual orientation and is minimized for configurations in which the molecules are aligned to a certain extent. As a result of the competition between orientation entropy and excluded volume effects, the system exhibits a first-order transition from an isotropic, through a biphasic, to an ordered phase. The critical boundaries are roughly inversely proportional to the excluded volume. In addition to the usual parameters controlling the phase transition (e.g., ionic strength, molecular weight, etc.), for su-

Submitted January 29, 2002, and accepted for publication April 22, 2002.

Address reprint requests to Dr. Johan R. C. van der Maarel, Gorlaeus Laboratories, Leiden University, P.O. Box 9502, 2300 RA Leiden, The Netherlands. Tel.: 31-71-5274543; Fax: 31-71-5274397; E-mail: j.maarel@chem.leidenuniv.nl.

0006-3495/02/08/1119/11 $2.00

percoiled DNA topology plays an important role. Apart from its effect on the molecular free energy, the topological constraint determines the total length and diameter of the superhelix, and hence, the volume excluded to another supercoil. Here, we will explore the major parameters controlling the formation of the ordered phase to gauge their significance and to understand how they operate.

The primary aim of the present communication is to investigate the nature of the phase transition and to characterize the liquid crystalline structure. For this purpose, we will present the phase diagram of pUC18 DNA with a moderate superhelical density $\sigma \approx -0.03$. The electrostatic interaction is modified by the ionic strength of the supporting medium. Critical phase boundaries are obtained from ^{31}P nuclear magnetic resonance (NMR) (Strzelecka and Rill, 1987), polarized light microscopy (Rill et al., 1991; Livolant and Leforestier, 1996), and macroscopic phase equilibrium experiments (Kassapidou et al., 1998). For the latter experiments, biphasic samples were prepared and the critical boundaries c_i and c_a were obtained by extrapolation to the concentrations at which the anisotropic phase first appears and the isotropic phase fully disappears, respectively. Polarized light microscopy is done to complement the presentation of the phase diagram and to characterize the liquid crystalline structure by its unique texture. Finally, at higher plasmid concentration, the latter technique will provide preliminary evidence for the formation of a true crystal.

The isotropic–anisotropic phase boundaries will be compared with theoretical predictions based on the coexistence equations, which are derived from the solution free energy including orientation entropy and excluded volume effects of semiflexible, wormlike particles (Onsager, 1949; Khokhlov and Semenov, 1981, 1982; Odijk, 1986; Stroobants et al., 1986). Because existing theory is strictly valid for particles with fixed molecular free energy, we have supplemented the solution free energy with the intramolecular elastic, entropic, and electrostatic free energy contributions pertaining to the supercoil (Marko and Siggia, 1995). With the wormlike cylinder as reference system, the intermolecular electrostatic contribution to the solution free energy is evaluated as a thermodynamic perturbation in the second virial approximation with a Debye-Hückel potential of mean force. Due to the moderate size of our plasmid (plectonemic length around 400 nm), the virial expansion for the reference system has to be carried to higher order. We have used Cotter's (1977) scaled particle theory, because its result improves significantly over the second virial approximation and compares favorably with many experimental results including the phase boundaries of short DNA fragment solutions (Sato and Teramoto, 1996; Kassapidou et al., 1998).

Topology

In the calculation of the phase boundaries, we will ignore branching of the supercoil and the possible formation of cruciform structures. The topology is important however, because it determines the physical size of the superhelix and the volume excluded to another supercoil. For a description of the topology, it is assumed that the double stranded DNA coil takes a helical configuration with radius r and pitch $2\pi p$. We let the helix be right-handed with a negative superhelical density $\sigma = \Delta Lk/Lk_0$, with excess linking number deficit ΔLk and Lk_0 being the linking number if the coil is fully relaxed. The excess linking number deficit is related to the writhing number Wr and the excess twist ΔTw according to

$$\Delta Lk = Wr + \Delta Tw \tag{1}$$

(White, 1969). For a right-handed, regular supercoil without end loops, the writhing number is simply proportional to the number of crossings n when viewed perpendicular to the superhelical axis $Wr = -n \sin \alpha$, with the plectonemic pitch angle α (Bloomfield et al., 2000). L denotes the total length of the supercoil projected on the superhelical axis. It is convenient to define the normalized length $2L/l$, with l being the DNA length measured along the contour. From integration along the contour, it follows that

$$2L/l = p/(p^2 + r^2)^{1/2} \tag{2}$$

if the end loops are neglected. The pitch angle α is given by

$$\tan \alpha = p/r = (2L/l)/(1 - (2L/l)^2)^{1/2} \tag{3}$$

and the writhing number reads

$$Wr = -lp/(2\pi(p^2 + r^2)) \tag{4}$$

The structure of the supercoil is hence fully characterized by the lengths l, p, and r. The pitch p and radius r determine the opening angle α, the writhe Wr, and the normalized length of the superhelical axis $2L/l$.

Phase boundaries

For the calculation of the interaction among supercoils, we model the supercoil as a uniformly charged semiflexible cylinder with plectonemic radius r and length L. For the time being, we ignore the molecular effects of the superhelical structure on the phase boundaries. The latter effects are important only if the plectonemic dimensions change through the phase transition and will be considered below. In the Debye-Hückel approximation, for two rod-like polyelectrolyte segments skewed at an angle ϕ the electrostatic potential has the form

$$w/(kT) = A \exp[-\kappa x]/\sin \phi \tag{5}$$

in which x denotes the shortest distance between the central axes (Brenner and Parsegian, 1974). For solutions in excess

simple salt with ionic strength I, the inverse screening length κ is given by $\kappa^2 = 8\pi QI$, with Bjerrum length $Q = e^2/(\varepsilon kT)$. The constant $A = 2\pi\bar{\nu}_{\text{eff}}^2 Q\kappa^{-1}$ depends on the effective number of charges per unit length along the superhelical axis $\bar{\nu}_{\text{eff}}$. For a line charge one simply has $\bar{\nu}_{\text{eff}} = Q^{-1}$, provided the charge is renormalized according to the condensation concept (Manning, 1969). Here, the effect of the finite radius of supercoil cannot be ignored and the effective charge density takes the form $\bar{\nu}_{\text{eff}} = [Q\kappa r K_1(\kappa r)]^{-1}$, with K_1 the first order modified Bessel function of the second kind. In the second virial approximation (for both electrostatic and hard-core interactions), the Helmholtz free energy of a solution of N polyelectrolytes is given by (Stroobants et al., 1986)

$$\Delta F/(NkT) = \text{constant} + \ln c_{\text{p}} + \sigma_{\text{E}} - c_{\text{p}}\langle\beta\rangle/2 \quad (6)$$

with σ_{E} the orientation entropy and c_{p} the rod number concentration N/V. For hard spherocylinders, Sato and Teramoto (1991) have derived an expression for the binary cluster integral with isotropic preaveraging of end effects

$$-\langle\beta\rangle/2 = \frac{\pi}{4}\left[L^2 D^{\text{eff}}\rho + \frac{L^2}{\kappa}\eta + 4L\bar{D}_{\text{eff}}^2\left(1 - \frac{4\Delta}{\pi\bar{D}_{\text{eff}}}\right) + \frac{8}{3}\bar{D}_{\text{eff}}^3\left(1 - \frac{3\pi\Delta}{2\bar{D}_{\text{eff}}} + 3\left(\frac{\Delta}{\bar{D}_{\text{eff}}}\right)^2\right)\right] \quad (7)$$

with

$$\Delta = [(2\ln 2)\bar{D}_{\text{eff}}/\kappa - (\ln 2)^2/\kappa^2]^{1/2} \quad (8)$$

and effective diameters

$$D^{\text{eff}} = 2r + \kappa^{-1}(\ln A' + \gamma + \ln 2 - 1/2) \quad (9)$$

$$\bar{D}_{\text{eff}} = 2r + \kappa^{-1}(\ln A' + \gamma - \ln 2 + 1) \quad (10)$$

in which γ denotes Euler's constant and $A' = A\exp(-2\kappa r)$. The parameters ρ and η are proportional to the orientation pair excluded volume. For the isotropic phase, these parameters take the values $\rho = 1$ and $\eta = 0$; in the liquid crystalline phase they depend on the orientation parameter α_{D} (Onsager, 1949; Stroobants et al., 1986). For the orientation entropy σ_{E} we use DuPré and Yang's (1991) modification of Odijk's (1986) expression, so as to agree with Khokhlov and Semenov's (1981, 1982) asymptotic limits of very flexible and very stiff wormlike chains,

$$\sigma_{\text{E}} = \ln \alpha_{\text{D}} - 1 + \pi e^{-\alpha_{\text{D}}} + (\alpha_{\text{D}} - 1)N_{\text{p}}/6 + 5\ln(\cosh((\alpha_{\text{D}} - 1)N_{\text{p}}/5))/12 \quad (11)$$

Here, σ_{E} has an explicit length dependence expressed as the number N_{p} of persistence length units per chain. With a bending persistence length of the supercoil $P_{\text{sc}} \approx 100$ nm, i.e., being twice the value of the persistence length of the duplex P_{b}, for pUC18 plasmid in the plectonemic form N_{p} is on the order of 4. In the anisotropic phase the orientation parameter α_{D} follows from minimization of the free energy $\partial\Delta F/\partial\alpha_{\text{D}} = 0$. Phase boundaries are obtained from the coexistence equations between the anisotropic and isotropic phases $\mu_{\text{i}} = \mu_{\text{a}}$ and $\Pi_{\text{i}} = \Pi_{\text{a}}$, with osmotic pressure $\Pi = -(\partial\Delta F/\partial V)_{\text{T,N},\mu_0}$ and chemical potential $\mu = -(\partial\Delta F/\partial N)_{\text{T,V},\mu_0}$.

For relatively stiff polyelectrolytes such as xanthan with large length over breadth aspect ratio, reasonable agreement with experimental data is observed when both the hard-core and electrostatic contributions are evaluated in the second virial approximation (Sato and Teramoto, 1996). However, pUC18 plasmid has a moderate molecular weight with aspect ratio of the supercoil on the order of 20 and the virial expansion for the reference system has to be carried to higher order. For this purpose, the hard-core reference part of the excluded volume (i.e., Eqs. 7–10 with zero screening length) is replaced by the relevant expressions given by scaled particle theory (Cotter, 1977). The electrostatic contribution is treated as a thermodynamic perturbation in the second virial approximation. Although for rodlike particles scaled particle theory lacks rigorous theoretical justification, its result improves significantly over the second virial expansion and compares favorably with experimental results including the critical boundaries of 150-bp DNA fragment solutions at sufficiently high salt concentration (Kassapidou et al., 1998). For an extensive description of scaled particle theory in the context of polymer liquid crystal formation the review papers by Sato and Teramoto (1991, 1996) may be consulted.

Effects of supercoiling

The above-delineated procedure for the calculation of the phase boundaries is strictly applicable for particles with constant molecular free energy. In the case of supercoils, the molecular free energy depends on the topology of the superhelix (Marko and Siggia, 1995). The topology may however be sensitive to intermolecular organization and solution structure. In our scattering work, the radius, pitch, and length of the superhelix were indeed seen to decrease significantly with increasing plasmid concentration prior and covering the transition to the liquid crystalline phase. Accordingly, we will supplement the solution free energy Eq. 6 with the molecular elastic, entropic, and electrostatic terms coming from the plectonemic structure listed below. These contributions are potentially important in controlling the phase boundaries through the balance of the chemical potentials pertaining to the coexisting phases.

The elastic contribution to the free energy of a supercoil per unit strand reads (Marko and Siggia, 1995)

$$F_{\text{elas}}/(kTl) = 1/2P_{\text{b}}\kappa_{\text{c}}^2 + 1/2P_{\text{t}}\Omega^2,$$

$$\kappa_{\text{c}} = r/(r^2 + p^2),$$

$$\Omega = 2\pi/l(\Delta Lk - Wr) \quad (12)$$

with P_b and P_t the bending and torsional persistence length of the DNA duplex, respectively. The curvature κ_c is expressed in terms of the plectonemic radius r and pitch p, and the excess twist Ω has been eliminated with White's Eq. 1. A given point on the supercoil has radial displacements of order r and displacements along the superhelical axis of order πp. The corresponding free energy of confinement per unit strand takes, hence, the form (Marko and Siggia, 1995; Burkhardt, 1995)

$$F_{conf}/(kTl) = 3/2^{8/3}(P_b^{-1/3}(\pi p)^{-2/3} + P_b^{-1/3}r^{-2/3}) \quad (13)$$

For the electrostatic contribution, we will use the approximate form for a superhelix with opening angle $\alpha > 45°$ immersed in a medium with inverse screening length κ (Ubbink and Odijk, 1999)

$$\frac{F_{elec}}{kTl} = \frac{1}{2}\nu_{eff}^2 Q\left[\frac{2\pi}{2}\right]^{1/2} \exp[-w]\left(1 + \frac{0.207}{\mu} + \frac{0.054}{\mu^2}\right),$$

$$w = 2\kappa r,\ \mu = p^2/4r^2 \quad (14)$$

Here, ν_{eff} is the effective number of charges per unit length of the DNA duplex and should not be confused with the corresponding parameter pertaining to the superhelix $\bar{\nu}_{eff}$. According to the condensation concept (Manning, 1969) and with bare diameter a, the effective charge density of the duplex takes the form $\nu_{eff} = [Q\kappa a K_1(\kappa\alpha)]^{-1}$.

A decrease in radius and/or pitch results in an increase in the elastic, entropic, and electrostatic molecular energy contributions. As we will see shortly, through the effect on the chemical potentials, this increase in molecular free energy generates a destabilization of the anisotropic phase, a broadening of the phase gap, and a shift of the critical boundary pertaining to the disappearance of the isotropic phase toward higher concentration.

MATERIALS AND METHODS

Isolation of pUC18 clone vector DNA

pUC18 plasmid (2686 base pairs) was prepared from *Escherichia coli* DH5α (Bhikhabhai et al., 2000). A colony was transformed with pUC18 and grown on a Luria Broth agar plate with ampicillin (100 μg/mL). A single colony was taken to grow a culture in Terrific Broth (TB) medium (12 g of tryptone, 24 g of yeast extract, 4 mL of glycerol, 2.3 g of KH_2PO_4, and 12.5 g of K_2HPO_4 per dm^3) and ampicillin at 37°C. After 7 h, this culture was put into a fermentor, which contained 30 dm^3 TB-medium, ampicillin, and an antifoam agent. The bacteria were cultured for 17 h at 37°C under continuous shaking, aeration, and, subsequently, harvested and stored at −20°C. The cells were suspended in TEG buffer (25 mM Tris, 10 mM EDTA, 50 mM glucose, pH 8) and lysed with an alkaline solution (0.2 M NaOH, 1% sodium dodecyl sulfate) at room temperature. Bacterial genomic DNA, cellular debris, and proteins were precipitated by the addition of 3 M potassium acetate at 4°C. After centrifugation, the supernatant was treated with 5 M ammonium acetate to precipitate any residual contaminants (Sun et al., 1994). RNA and protein were removed with rnase (20 μg/mL, 37°C, 1 h) and proteinase K (100 μg/mL, 55°C, 1 h) treatments, respectively. After precipitation with cold isopropanol, the DNA pellet was dried for a short period and dissolved in TE buffer (10 mM Tris, 1 mM EDTA, pH 8) for storage at 4°C. The advantage of this procedure is that it has a high yield of typically 75 mg of plasmid DNA per isolation using 4 of 30 dm^3 cell culture.

Plasmid characterization, purification, and sample preparation

The integrity of the plasmid was checked with 1% agarose gel electrophoresis in Tris-acetate buffer (40 mM Tris-acetate, 2 mM EDTA, pH 8.3) at 75 V for 1 h (Backendorf et al., 1989). The linking number deficit and the percentage of open circular DNA were determined by 1.4% agarose gel electrophoresis in the same buffer but with 10 μg/mL chloroquine at 50 V for 17 h (van Workum et al., 1996). Apart from supercoiled DNA, an isolated batch contained some chromosomal DNA and a small amount of aggregated plasmid. The topoisomer distribution is characterized by predominant linking number deficit $\Delta Lk = -7 \pm 3$, which corresponds with a superhelical density $\sigma = -0.03$ (for chloroquine-free pUC18 $Lk_0 = 262$). Gel electrophoresis showed that less than 5% of plasmids are nicked and open circular. Furthermore, the ratio of the optical absorbencies $A_{260}/A_{280} = 1.83$ indicates that the material is also free of protein and RNA. The hypochromic effect at 260 nm (>35%) confirms the integrity of the duplex. For sample preparation, the purified plasmids were precipitated in ethanol and the 10% residual water content in the gently dried pellet was determined with infrared spectroscopy. The pellet was subsequently dissolved in NaCl solutions and the DNA concentration was determined by weight and checked with ultraviolet spectroscopy.

NMR, polarized light microscopy, and phase separation experiments

The NMR experiments were done with a Bruker AM-200 spectrometer equipped with a 4.7-T wide-bore superconducting magnet. Spectra were obtained after Fourier transformation of the free induction decay following a single 8.5-μs excitation pulse. Typically, 64-K scans with a bandwidth of 5 kHz and a relaxation delay of 1 s were collected overnight. The samples were prepared in 0.1 M NaCl with DNA concentrations 3.8, 4.8, 6.0, 7.7, 14, and 30 g/dm^3 and they were contained in nonspinning 5-mm outer diameter glass tubes. The temperature was controlled at 298 K, and the samples were allowed to equilibrate for at least 1 h before the spectrum was taken. For polarized microscopy, samples were prepared in 0.1 M NaCl with DNA concentrations 5, 15, 25, and 30 g/dm^3. A droplet was deposited and sealed between slide and coverslip with a 50-μm polyethylene terephthalate spacer and observed with a Leica DMR microscope with 63× and 100× (oil immersion) objectives at ambient temperature. The magnification factors were calibrated with the help of a ruler. To induce macroscopic alignment of the cholesteric axis, samples were exposed overnight to a strong 14-T NMR magnetic field so that the direction of the magnetic field is parallel to the slide. For phase separation experiments, in 5-mm inner diameter glass tubes samples were prepared in a concentration range between 1 and 30 g DNA/dm^3 in 5, 8, 10, 20, 40, 60, 100, 200, 400, and 600 mM NaCl. Phase separation took place over periods from a couple of days to 4 weeks for samples with low amounts of added salt. Due to the significant difference in DNA density, the liquid crystalline phase settles at the bottom of the tube. The volume ratio of the respective isotropic and liquid crystalline phases was measured with a cathetometer (Wilt M 10) as a function of the total DNA concentration. The temperature was controlled at 298, 308, and 328 K by immersion of the sample tubes in a water bath.

RESULTS

^{31}P NMR spectroscopy

If the plasmid concentration is increased beyond a certain critical concentration, the translucent solution is seen to be

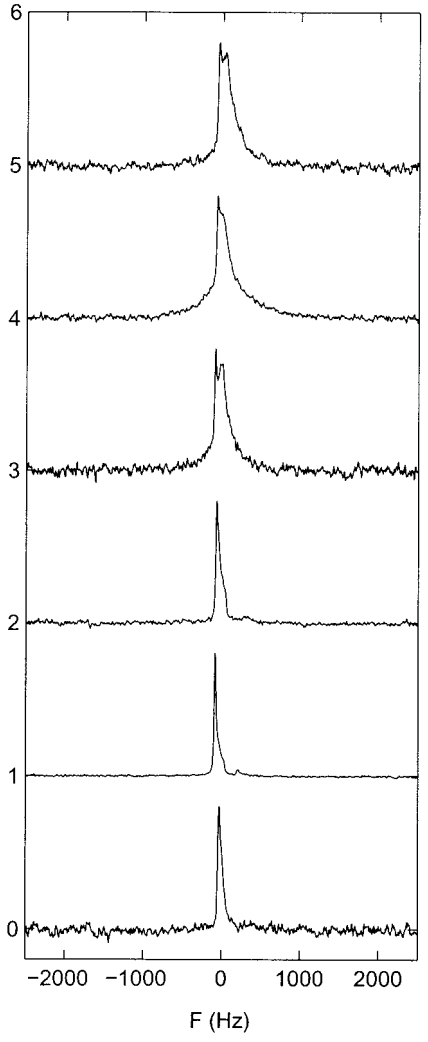

FIGURE 1 Normalized ^{31}P NMR spectra of supercoiled pUC18 DNA solutions (T = 298 K). All spectra were acquired with a bandwidth of 5 kHz. The average DNA concentration is from bottom to top: 3.8, 4.8, 6.0, 7.7, 14, and 30 g of DNA/dm^3.

composed of birefringent domains when observed through crossed polarizers. Polarized light microscopy shows that this behavior is due to the formation of an anisotropic liquid crystalline phase, rather than aggregation phenomena. In solutions containing linear DNA, the formation of an anisotropic phase results in a broadening of the ^{31}P NMR spectra due to incomplete averaging of the chemical shift anisotropy at a time scale of the inverse Larmor frequency (Strzelecka and Rill, 1987; Rill et al., 1991). The appearance of an isotropic phase is hence easily detected by the emergence of a relatively narrow ^{31}P resonance.

^{31}P NMR spectra of supercoiled pUC18 DNA solutions in 0.1 M NaCl are displayed in Fig. 1. Generally, they exhibit a narrow resonance superposed on a broad component originating from the anisotropic phase. The broad component is asymmetrically dispersed about the narrow resonance due to the chemical shift anisotropy (Shindo et al., 1980). These results are very similar to the ones reported for 150-bp fragments (Strzelecka and Rill, 1987). For a plasmid concentration as low as 3.8 g DNA/dm^3, the ^{31}P resonance is still narrow, but at slightly higher plasmid concentrations a progressive growth of a broadened signal contribution is observed. This growth saturates for concentrations exceeding, say, 14 g DNA/dm^3, but even at the highest investigated concentration with 30 g DNA/dm^3 a small contribution coming from the isotropic phase is still discernible. The observation of coexisting phases and the progressive growth of the broad component with increasing DNA concentration comply with a first order phase transition. More convincing evidence for a first order transition will be presented below, when the results of macroscopic phase equilibrium experiments are discussed. Furthermore, from the latter experiments, we can more accurately estimate the critical boundary concentrations pertaining to the first appearance of the anisotropic phase and disappearance of the isotropic phase, c_i and c_a, respectively. At 298 K and in 0.1 M NaCl, the boundaries are $c_i = 3$ and $c_a = 15$ g DNA/dm^3 (see below). In particular, the low value for c_i is in good agreement with the concentration dependence of the narrow component in the ^{31}P spectra. The observation that the growth of the broad component saturates for concentrations exceeding 14 g DNA/dm^3 is also in agreement with the phase separation value for c_a, but the fact that for higher concentrations the narrow signal persists indicates the presence of some residual isotropic phase immersed in the liquid crystal. We will now first discuss polarized light microscopic observations to characterize the liquid crystalline structures and to complement the presentation of the phase diagram.

Polarized light microscopy

Observations with polarized light microscopy confirm the existence of cholesteric germs in solutions with plasmid concentration 5 g DNA/dm^3 (Fig. 2 *a*). The germs appear as irregular spheres with a diameter on the order of 15 μm and they exhibit blue and yellow interference colors generated by a full-wave retardation plate. The molecules are aligned parallel to the interface between the isotropic and liquid crystalline phase. In the radial direction away from the center, the germs show a periodicity with alternation of dark and light stripes corresponding to half the cholesteric pitch. The pitch is 5 μm, which is about twice the value reported for the cholesteric phase of short fragment DNA (Brandes and Kearns, 1986; Rill et al., 1991; Livolant and Leforestier, 1996).

When the plasmid concentration is raised to 15 g DNA/dm^3, the solution becomes completely liquid crystalline. However, the characterization of the liquid crystalline phase is somewhat problematic, because nonaligned samples do not show the characteristic fingerprint-like textures ex-

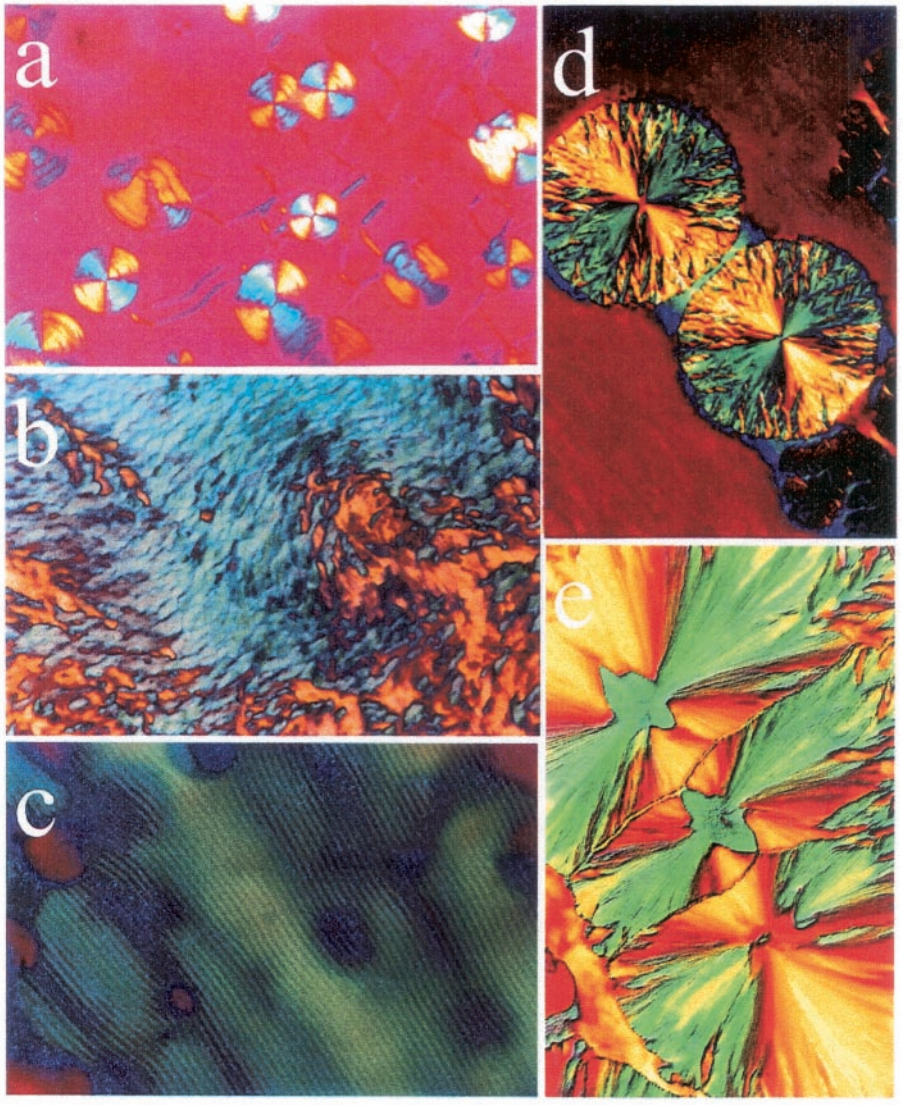

FIGURE 2 Polarized light microscopy textures of supercoiled pUC18 DNA in 0.1 M NaCl. (*a*) Cholesteric spherulites immersed in isotropic phase, 5 g of DNA/dm^3, 1000×; (*b*) nonaligned cholesteric phase, 15 g of DNA/dm^3, 1000×; (*c*) same as in *b* but after prolonged exposure to a 14-T magnetic field; (*d*) spherulites of supercoiled DNA in a crystalline state, 25 g of DNA/dm^3, 630×; (*e*) merged crystalline spherulites, 30 g of DNA/dm^3, 1000×.

pected for a cholesteric molecular organization (Fig. 2 *b*). This has caused some confusion in the literature concerning the assignment of the liquid crystalline phase (Torbet and DiCapua, 1989; Reich et al., 1994). Due to the negative diamagnetic susceptibility of the bases, DNA tends to arrange with its long axis perpendicular to the direction of a magnetic field (Maret et al., 1975). For linear DNA, this effect can be used to induce macroscopic alignment of the cholesteric axis (Brandes and Kearns, 1986; Groot et al., 1994; Kassapidou et al., 1995). However, supercoiled DNA has a very weak diamagnetic anisotropy, because the axis of the double helix follows a classical plectonemic trajectory such that the anisotropy of the bases averages out (Torbet and DiCapua, 1989). We have succeeded in inducing macroscopic alignment by exposing the preparation slide for more than 12 h in a 14-T field generated by a superconducting magnet. As displayed in Fig. 2 *c*, typical cholesteric, fingerprint-like textures are now observed, provided the direction of the magnetic field was parallel to the slide so that the cholesteric axis is oriented perpendicular to the line of view. The cholesteric pitch, measured for twice the distance between the fringes, amounts 4 μm, which is close to the value observed in the cholesteric germs at lower plasmid concentration (5 μm).

At higher plasmid concentration 25 g DNA/dm^3, a remarkable phenomenon occurs: formation of crystalline spherulites showing a well-defined Maltese cross and regular structure (Fig. 2 *d*). These textures are very different from those reported for the high density, liquid crystalline phases of linear DNA such as the columnar hexagonal phase

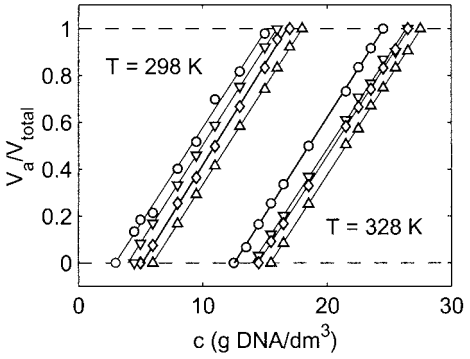

FIGURE 3 Liquid-crystalline volume fraction versus average DNA concentration in biphasic pUC18 solutions ($\sigma = -0.03$), (○): 0.1 M; (▽): 0.2 M; (◇: 0.4 M; (△), 0.6 M NaCl. The lines represent least-squares fits to extrapolate to the critical boundaries c_i and c_a, i.e., the concentration at which the anisotropic phase first appears and the isotropic phase disappears, respectively.

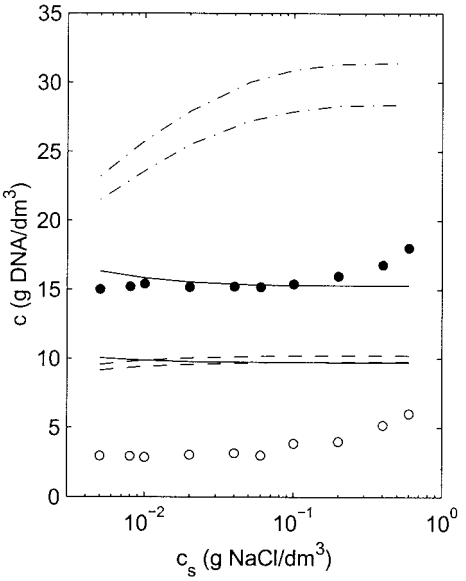

FIGURE 4 Critical boundaries pertaining to the isotropic-cholesteric phase transition versus the concentration added salt ($T = 298$ K). Open symbols, c_i; closed symbols, c_a. The dashed-dotted curves are calculated with hard-core and electrostatic interactions in the second virial approximation; $r_i = r_a = 10$ nm, $\alpha_i = \alpha_a = 65°$. The other curves are calculated with the scaled particle description for hard-core effects and electrostatic interactions in the second virial approximation; dashed curves, $r_i = r_a = 10$ nm, $\alpha_i = \alpha_a = 65°$; solid curves, $r_i = 10$ nm, $\alpha_i = 65°$, $r_a = 7.5$ nm, $\alpha_a = 58°$.

(Rill et al., 1991; Livolant and Leforestier, 1996). As far as we are aware, the observation of crystalline spherulites is unprecedented for both linear and supercoiled DNA in aqueous solution at comparable DNA concentration and/or levels of hydration. The diameter of the spherulites is on the order of 80 μm, which is a factor of 5 larger than the size of the cholesteric germs observed at lower concentration. They exhibit blue and yellow interference colors generated by a full-wave retardation plate in the same manner as the cholesteric germs, which suggest that the DNA molecules are oriented perpendicular to the spherulite radius. However, in contrast to the cholesteric germs they do not exhibit a periodicity in the radial direction, so there is no twist with increasing distance away from the center. As displayed in Fig. 2 *e*, at the highest investigated concentration 30 g DNA/dm^3, the spherulites merge. The merging of the spherulites indicates that their structure is rather soft and deformable. However, the characterization of the high density, true crystalline phase is beyond the scope of the present communication, and we will further focus on the transition between the isotropic and cholesteric phase.

Phase separation experiments

For macroscopic phase separation experiments, biphasic samples with coexisting cholesteric and isotropic phases were prepared. As shown in Fig. 3, the volume fraction of the anisotropic phase increases linearly from zero for isotropic samples to unity for the liquid crystal. The transition is indeed strongly first-order with a rather broad gap between the isotropic and liquid crystalline phases. At 298 K, the extrapolated concentrations at which the anisotropic phase first appears and the isotropic phase completely disappears, respectively, are rather low and agree with the ones inferred from ^{31}P NMR. The extrapolated boundaries are displayed in Fig. 4 as a function of the supporting salt concentration. For concentrations below, say, 0.1 M NaCl, the boundaries are rather salt concentration independent, for higher salt concentrations they show a small increase with increasing ionic strength. This behavior is very different from the one observed for 150-bp linear fragments, where the phase diagram shows a relatively narrow phase gap in the concentration range 100 to 225 g DNA/dm^3. Furthermore, the phase boundaries of linear DNA are strongly dependent on ionic strength (Kassapidou et al., 1998). For supercoiled DNA, the boundary concentrations are significantly lower than the limiting values pertaining to linear DNA in 0.1 M NaCl with comparable length 490 nm, i.e., $c_i = 13$ and $c_a = 67$ g DNA/dm^3 (for long, linear DNA the critical boundaries reach a plateau when the contour length exceeds 190 nm; Merchant and Rill, 1997).

In contrast to the weak salt dependence, the phase boundaries of supercoiled pUC18 DNA are very sensitive to temperature. The temperature-dependent phase diagram is depicted in Fig. 5. At a sufficiently high, fixed DNA concentration, it is possible to convert the anisotropic into the isotropic phase by raising the temperature; the liquid crystal reappears once the solution is cooled below the clearing point. We have checked that this clearing effect is fully reversible, so there are no irreversible changes in DNA primary structure such as melting of the duplex involved. The clearing point depends on overall plasmid concentra-

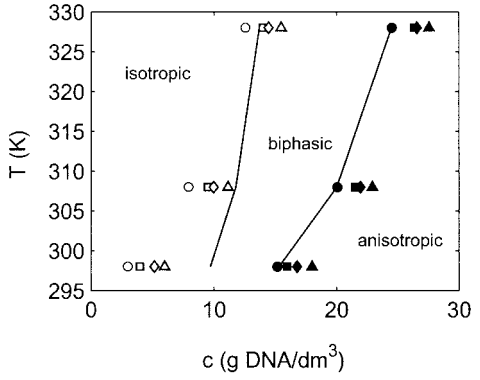

FIGURE 5 Temperature dependent phase diagram of pUC18 DNA solutions ($\sigma = -0.03$). (○): 0.1 M; (▽): 0.2 M; (◇): 0.4 M; (△), 0.6 M NaCl. Open symbols, c_i, closed symbols, c_a. The lines connect the theoretical phase boundaries calculated with $r_i = 10$, 9.4, and 8.9 nm with $\alpha_i = 65°$; $r_a = 7.5$, 6.9, and 6.4 nm with $\alpha_a = 58°$ for $T = 298$, 308, and 328 K, respectively.

TABLE 1 Parameter values used in the calculation of the phase boundaries pUC18 DNA

Supercoil radius isotropic phase	r_i	10 nm;* 9.4 nm;† 8.9 nm†
Supercoil radius anisotropic phase	r_a	7.5 nm;* 6.9 nm;† 6.4 nm†
Opening angle isotropic phase	α_i	65°*
Opening angle anisotropic phase	α_a	58°*
Linking number deficit	ΔLk	−7
Supercoil bending persistence length	P_{sc}	100 nm
Duplex bending persistence length	P_b	50 nm
Duplex torsional persistence length	P_t	75 nm
Duplex contour length	l	920 nm
Duplex bare diameter	a	2 nm
Bjerrum length	Q	0.71 nm

*Experimental values estimated by SANS; the values refer to plasmid concentration 3 and 15 g/dm^3 for the isotropic and anisotropic phase, respectively.
†Optimized values to satisfy the observed temperature dependence of c_a.

tion as shown in Fig. 5. For pBluescript plasmid (2960 bp) at concentrations of 10 to 25 g DNA/dm^3, Reich et al. (1994) have reported a clearing point at 351 K, which is in good agreement with our data. The temperature dependence of the phase diagram is very different from the one observed for 50-nm length linear DNA, where the boundaries were observed to be weakly dependent on temperature only (Strzelecka and Rill, 1987).

DISCUSSION

The experimental results can be explained by considering the interplay between excluded volume and orientation order. To decrease excluded volume, the system increases anisotropy with a concurrent decrease in physical extent of the supercoil. The latter effect is unique for topologically constrained polymer and has been inferred from an analysis of the SANS structure factor. Branching is also potentially important in controlling the physical extent of the superhelix. In our scattering work, effects of branching were beyond observation, however, because in the used range of momentum transfer interference over a spatial extent on the order of the radius and pitch of the superhelix was sampled. In the liquid crystal, branching of the superhelix is presumably suppressed due to the spatial confinement, but in the more diluted, isotropic phase it can have a significant effect on the excluded volume. In the theoretical analysis, however, we will neglect branching as analytic expressions describing its effect on the phase boundaries are not available.

The boundary concentrations are calculated with the coexistence equations, which are derived from the solution free energy including orientation entropy and excluded volume. With a bending persistence length of the supercoil on the order of 100 nm, the orientation entropy is close to the one for very flexible chains and effects of overall flexibility on the phase behavior are expected to be moderate. The virial terms are calculated with the assumption that the intermolecular interactions are a sum of hard-core and electrostatic interactions. The electrostatic potential is obtained from the linearized version of the Poisson-Boltzmann equation for cylindrical polyelectrolytes with excess salt (Debye-Hückel approximation). Due to counterion condensation (Manning, 1969), the net effective charge of the supercoil is quite moderate, which results in a fairly weak electrostatic interaction. This is illustrated by the value of the effective diameter according to Eq. 9, which amounts 21 nm only for a superhelix with bare plectonemic diameter 20 nm in 0.05 M NaCl. With the wormlike cylinder as reference system, the electrostatic contribution to the free energy is evaluated as a thermodynamic perturbation in the second virial approximation (Sato and Teramoto, 1991). The hard-core contribution has either been evaluated in the second virial approximation or with scaled particle theory to include higher order terms (Cotter, 1977).

Parameters used in the calculation of the phase boundaries are collected in Table 1. The relevant dimensions of the supercoil (i.e., radius and opening angle) were experimentally derived with SANS (for 298 K only). The predominant linking number deficit was obtained by band counting in gel electrophoresis and the bending and torsional persistence lengths were taken from the literature (Bloomfield et al., 2000). There are no adjustable parameters.

The dashed-dotted curves in Fig. 4 represent the c_i and c_a calculated with both the hard-core and electrostatic interactions in the second virial approximation. We have first assumed that the plectonemic dimensions do not change through the phase transition, i.e., the boundaries were calculated with the entries in Table 1 pertaining to the isotropic phase. Under this condition, the molecular free energy is irrelevant in the balance of chemical potentials and, accordingly, we obtain the conventional moderate phase gap be-

tween the isotropic and anisotropic phase (Onsager, 1949; Odijk, 1986). Second virial theory does not correctly predict the width of the phase gap, overestimates the boundaries, and predicts a too steep dependence on the supporting electrolyte concentration. Similar behavior has previously been observed for 150-bp DNA fragments in saline solutions (Kassapidou et al., 1998). It is clear that the virial expansion of the hard-core reference system has to be carried to higher order.

The dashed curves in Fig. 4 are calculated with the scaled particle description of hard-core effects and electrostatic interactions in the second virial approximation. Again, we did not include a possible change in plectonemic dimensions through the phase transition. The scaled particle description represents a significant improvement over the second virial expansion in the sense that the theoretical predictions are now right between the experimental boundaries. However, this approach still fails to reproduce the width of the phase gap. The theoretical predictions can be improved if the dimensions of the supercoil are allowed to change through the phase transition in a manner consistent with the interpretation of neutron scattering data reported in the accompanying paper.

Finally, we have allowed for a decrease in radius and opening angle if the supercoil is confined in the anisotropic phase. Due to the decrease in excluded volume and increase in molecular free energy, the theoretical prediction for the critical boundary pertaining to the disappearance of the isotropic phase (c_a) is shifted toward higher packing fraction. The prediction for the critical boundary at which the anisotropic phase first appears (c_i) is unaffected, because the dimensions in the isotropic phase were kept at their original values. In the calculation, we have used an ionic strength independent radius of the supercoil. The little increase in predicted critical concentrations at low ionic strength is due to the electrostatic contribution to the molecular free energy. The latter contribution becomes more important under minimal screening conditions, but its effect is vanishing small for supporting salt concentrations exceeding, say, 0.05 M.

As can be seen in Fig. 4 (solid curves), c_a is now in reasonable agreement with the experimental data. The boundary pertaining to the first appearance of the anisotropic phase c_i is still not correctly reproduced, despite that the theoretical phase gap is now significantly broadened. In principle, the low value for c_i can be accounted for by assuming an even larger value of the plectonemic radius in the isotropic phase. However, due to the already very open structure of the superhelix, we consider a radius exceeding the measured SANS value 20 nm (in 0.05 M NaCl) unlikely. Another explanation for the low c_i can be found in branching of the superhelix. In the liquid crystal, branching is presumably suppressed due to the spatial confinement, but in the more diluted, isotropic phase it can significantly increase the excluded volume. As a result of this increase in excluded volume, the corresponding critical boundary is shifted toward lower packing fractions. Unfortunately, quantitative theory describing this effect is not available in the literature.

As seen in Fig. 4, the experimental critical boundaries are fairly insensitive to salt concentration and show a small increase for very high ionic strength ($>$0 1 M NaCl) only. An increase in plectonemic radius with decreasing ionic strength below, say, 0.1 M NaCl was observed with cryo-electron microscopy (Bednar et al., 1994), atomic force microscopy in situ (Lyubchenko and Shlyakhtenko, 1997; Cherny and Jovin, 2001), sedimentation and catenation experiments (Rybenkov et al., 1997a,b), SANS (Hammermann et al., 1998), as well as computer simulations (Gebe et al., 1996; Klenin et al., 1998). Our results show that for a plasmid with superhelical density around -0.03 the excluded volume, and, hence, physical extent of the superhelix are relatively constant over a range 0.005 to 0.1 M NaCl. This is probably related to the fact that in 0.05 M NaCl the radius is $\sim$20 nm and an even more open structure for lower salt concentrations seems to be unlikely. The small increase in critical boundaries for ionic strengths exceeding 0.1 M can be rationalized by a small decrease in plectonemic radius and/or decrease in helical repeat distance of the duplex. The latter effect results in an increase in number of (negative) superhelical turns and, consequently, a more tightly interwound configuration and smaller excluded volume.

With increasing temperature, the boundaries are also seen to shift to higher concentrations. It was checked that this behavior could not be reproduced by a reasonable decrease in overall bending rigidity of the superhelix, which suggests that the excluded volume decreases. Indeed, the observed shift of the boundaries can be reproduced by a small decrease in plectonemic radius and/or normalized length. The solid lines in Fig. 5 connect the phase boundaries calculated with the scaled particle description of hard-core effects and electrostatic interactions in the second virial approximation. Here, the plectonemic radii were optimized (at elevated temperatures only) so that the experimental c_a is reproduced. The optimized values are collected in Table 1. In this procedure, the *absolute* difference in radii pertaining to the isotropic and anisotropic phases was fixed at the original value (2.5 nm) so that the *relative* difference increases with increasing temperature. This results in an enhanced imbalance in molecular free energy and a widening of the phase gap. Furthermore, the theoretical predictions for c_i approach the experimental values, and at 328 K there is reasonable agreement.

However, it should be noted that the observed temperature behavior of the phase boundaries is at odds with the expected temperature behavior of the linking number deficit. With an increase in temperature, the helical repeat distance of the duplex increases, which results in a less tightly interwound configuration (this is the inverse of the effect of the ionic strength; Depew and Wang, 1975). As a

result of this decrease in winding of the superhelix, we expect the excluded volume to increase, which should shift the boundaries to lower concentration.

A plausible explanation for the thermal phase diagram can be found in a change in flexibility of the duplex and/or premelting effects. The compaction of negatively supercoiled DNA results in a decrease in physical size of the plectoneme at the cost of a positive twist exerted on the duplex, as suggested by the SANS data. Furthermore, if the twist exceeds a certain critical value, the torsion may be partially relaxed with the phosphate backbone turned inside and the unpaired bases exposed on the outside (Strick et al., 1998). With an increase in temperature, the flexibility increases due to increased breathing and/or premelting of the base pairs starting in adenine thymine-rich regions. As a consequence of the associated decrease in elastic energy, the superhelix can be more tightly interwound, which results in a smaller excluded volume and a reversible shift of the phase boundaries toward higher packing fractions.

CONCLUSIONS

^{31}P NMR, polarized light microscopy, and phase separation experiments show that supercoiled DNA spontaneously orders in a liquid crystalline phase if the plasmid concentration is increased beyond a certain critical value. The transition is strongly first-order with a rather broad phase gap between the isotropic and liquid crystalline phases. The critical boundaries are low compared with the ones pertaining to linear DNA with comparable contour length. Furthermore, they are strongly and reversibly dependent on temperature and weakly dependent on ionic strength. The liquid crystalline phase has unambiguously been assigned cholesteric with a pitch on the order of 4 μm. Due to the weak diamagnetic susceptibility, macroscopic alignment can only be achieved if the liquid crystal is exposed to a rather intense magnetic field strength for several hours. The pitch is about twice the value reported for the cholesteric phase of short fragment DNA; the increase in cholesteric pitch can be rationalized if one compares the shallow opening angle of the DNA duplex in the B-form (30°) to the one pertaining to the supercoil (~60°). Preliminary results show that at higher concentrations on the order of 25 to 30 g of DNA/dm^3 a true crystal is formed.

Supercoiling is a major factor in controlling the macroscopic phase boundaries, as suggested by the observed difference in phase behavior compared with linear DNA with similar length, the strong and reversible temperature dependence of the critical boundaries, and the weak dependence on the ionic strength. The latter behavior reflects that the electrostatic interactions are screened over a distance on the order of the plectonemic diameter so that the supercoils do not interact too strongly. This point of view is also supported by the scattering results; the structure factor of supercoiled pUC18 DNA in 0.05 M NaCl could be satisfactorily described with interactions among supercoils in the second virial approximation. The broadening of the phase gap can be partially explained by lyotropic liquid crystal theory including an increase in molecular free energy associated with a decrease in effective radius and length of the supercoil through the phase transition. For the critical boundary pertaining to the disappearance of the isotropic phase (c_a) the agreement is gratifying. However, theory fails to predict the low boundary concentrations at which the anisotropic phase first appears (c_i), although the agreement improves with increasing temperature. Of course, this behavior can be attributed to deficiencies in the theory, but a more obvious explanation can be found in branching of the superhelix. The reversible shift of the phase boundaries toward higher concentration with increasing temperature is probably related to the twist energy storing properties of the supercoil and changes in flexibility of the duplex due to increased breathing and/or premelting of the base pairs starting in AT-rich regions.

We thank Jacky Snoep, Coen van der Weijden, Hans den Dulk, and Tineke de Ruijter for assistance with gel electrophoresis and biochemical preparation procedures.

REFERENCES

Backendorf, C., R. Olsthoorn, and P. van de Putte. 1989. Superhelical stress restrained in plasmid DNA during repair synthesis initiated by the UvrA, B-protein and C-proteins in vitro. *Nucleic Acids Res.* 17: 10337–10351.

Bates, A. D., and A. Maxwell. 1993. DNA Topology. Oxford University Press, Oxford.

Bednar, J., P. Furrer, A. Stasiak, J. Dubochet, E. H. Egelman, and A. D. Bates. 1994. The twist, writhe and overall shape of supercoiled DNA change during counterion-induced transition from a loosely to a tightly interwound superhelix: possible implications for DNA structure in vivo. *J. Mol. Biol.* 235:825–847.

Bhikhabhai, R., M. Ollivier, and F. Blanche. 2000. A novel, rapid process for purification of plasmid for gene therapy. *Life Sci. News.* 5:1–4.

Bloomfield, V. A., D. M. Crothers, and I. Tinico, Jr. 2000. Nucleic Acids, Structures, Properties, and Functions. University Science Books, Sausalito, CA.

Brandes, R., and D. R. Kearns. 1986. Magnetic ordering of DNA liquid crystals. *Biochemistry.* 25:5890–5895.

Brenner, S. L., and V. A. Parsegian. 1974. A physical method for deriving the electrostatic interaction between rodlike polyions at mutual angles. *Biophys. J.* 14:327–334.

Burkhardt, T. W. 1995. Free energy of a semiflexible polymer confined along an axis. *J. Phys. A Math. Gen.* 28:L629–L635.

Cherny, D. I., and T. M. Jovin. 2001. Electron and scanning force microscopy studies of alterations in supercoiled DNA tertiary structure. *J. Mol. Biol.* 313:295–307.

Cotter, M. A. 1977. Hard spherocylinders in an anisotropic mean field: a simple model for a nematic liquid crystal. *J. Chem. Phys.* 66: 1098–1106.

Depew, R. E., and J. C. Wang. 1975. Conformational fluctuations of DNA helix. *Proc. Natl. Acad. Sci. U.S.A.* 72:4275–4279.

DuPré, D. B., and S. Yang. 1991. Liquid crystalline properties of solutions of persistent polymer chains. *J. Chem. Phys.* 94:7466–7477.

Gebe, J. A., J. J. Delrow, P. J. Heath, B. S. Fujimoto, D. W. Stewart, and J. M. Schurr. 1996. Effects of Na^+ and Mg^{2+} on the structures of

supercoiled DNAs: comparison of simulations with experiments. *J. Mol. Biol.* 262:105–128.

Groot, L. C. A., M. E. Kuil, J. C. Leyte, J. R. C. van der Maarel, R. K. Heenan, S. M. King, and G. Jannink. 1994. Neutron scattering experiments on magnetically aligned liquid crystalline DNA fragment solutions. *Liquid Crystals.* 17:263–276.

Hammermann, M., N. Brun, K. V. Klenin, R. May, K. Toth, and J. Langowski. 1998. Salt-dependent DNA superhelix diameter studied by small angle neutron scattering measurements and Monte-Carlo simulations. *Biophys. J.* 75:3057–3063.

Kassapidou, K., R. K. Heenan, W. Jesse, M. E. Kuil, and J. R. C. van der Maarel. 1995. Effects of ionic strength on the supramolecular structure in liquid crystalline solutions of persistent length DNA fragments. *Macromolecules.* 28:3230–3239.

Kassapidou, K., W. Jesse, J. A. P. P. van Dijk, and J. R. C. van der Maarel. 1998. Liquid crystal formation in DNA fragment solutions. *Biopolymers.* 46:31–37.

Khokhlov, A. R., and A. N. Semenov, A. N. 1981. Liquid-crystalline ordering in the solution of long persistent chains. *Phys. A.* 108:546–556.

Khokhlov, A. R., and A. N. Semenov. 1982. Liquid-crystalline ordering in the solution of partially flexible maromolecules. *Phys. A.* 112:605–614.

Klenin, K., H. Merlitz, and J. Langowski. 1998. A Brownian dynamics program for the simulation of linear and circular DNA and other wormlike chain polyelectrolytes. *Biophys. J.* 74:780–788.

Livolant, F., and A. Leforestier. 1996. Condensed phases of DNA: structures and phase transitions. *Prog. Polym. Sci.* 21:1115–1164.

Lyubchenko, Y. L., and L. S. Shlyakhtenko. 1997. Visualization of supercoiled DNA with atomic force microscopy in situ. *Proc. Natl. Acad. Sci. U.S.A.* 94:496–501.

Manning, G. S. 1969. Limiting laws and counterion condensation in polyelectrolyte solutions: I. Colligative properties. *J. Chem. Phys.* 51: 924–933.

Maret, G., M. V. Schickfus, A. Mayer, and K. Dransfeld. 1975. Orientation of nucleic acids in high magnetic fields. *Phys. Rev. Lett.* 35:397–400.

Marko, J. F., and E. D. Siggia. 1995. Statistical-mechanics of supercoiled DNA. *Phys. Rev. E.* 52:2912–2938.

Merchant, K., and R. L. Rill. 1997. DNA length and concentration dependencies of anisotropic phase transitions of DNA solutions. *Biophys. J.* 73:3154–3163.

Odijk, T. 1986. Theory of lyotropic polymer liquid crystals. 1986. *Macromolecules.* 19:2313–2328.

Onsager, L. 1949. The effects of shape on the interaction of colloidal particles. *Ann. N.Y. Acad. Sci.* 51:627–659.

Reich, Z., E. J. Wachtel, and A. Minsky. 1994. Liquid-crystalline mesophases of plasmid DNA in bacteria. *Science.* 264:1460–1463.

Rill, R. L., T. E. Strzelecka, M. W. Davidson, and D. H. van Winkle. 1991. Ordered phases in concentrated DNA solutions. *Phys. A.* 176:87–116.

Rybenkov, V. V., A. V. Vologodskii, and N. R. Cozzarelli. 1997a. The effect of ionic conditions on the conformations of supercoiled DNA: I. Sedimentation analysis. *J. Mol. Biol.* 267:299–311.

Rybenkov, V. V., A. V. Vologodskii, and N. R. Cozzarelli. 1997b. The effect of ionic conditions on the conformations of supercoiled DNA: II. Equilibrium catenation. *J. Mol. Biol.* 267:312–323.

Sato, T., and A. Teramoto. 1991. Perturbation theory of isotropic-liquid-crystal phase equilibria in polyelectrolyte solutions. *Phys. A.* 176:72–86.

Sato, T., and A. Teramoto. 1996. Concentrated solutions of liquid-crystalline polymers. *Adv. Polym. Sci.* 126:85–161.

Shindo, H., J. B. Wooten, B. H. Pheiffer, and S. B. Zimmerman. 1980. Nonuniform backbone conformation of deoxyribonucleic acid indicated by phosphorus-31 nuclear magnetic resonance chemical shift anisotropy. *Biochemistry.* 19:518–526.

Strick, T. R., J. F. Allemand, D. Bensimon, and V. Croquette. 1998. Behavior of supercoiled DNA. *Biophys. J.* 74:2016–2028.

Stroobants, A., H. N. W. Lekkerkerker, and T. Odijk. 1986. Effect of electrostatic interaction on the liquid crystal phase transition of rodlike polyelectrolytes. *Macromolecules.* 19:2232–2238.

Strzelecka, T. E., and R. L. Rill. 1987. Solid state ^{31}P NMR studies of DNA liquid crystalline phases: the isotropic to cholesteric transition. *J. Am. Chem. Soc.* 109:4513–4518.

Sun, N., B. Chen, J. Zhou, J. Yuan, X. Xu, D. Zhu, and K. Han. 1994. An efficient method for large-scale isolation of plasmid DNAs by heat-alkali co-denaturation. *DNA Cell Biol.* 13:83–86.

Torbet, J., and E. DiCapua. 1989. Supercoiled DNA is interwound in liquid-crystalline solutions. *EMBO J.* 8:4351–4356.

Ubbink, J., and T. Odijk. 1999. Electrostatic-undulatory theory of plectonemically supercoiled DNA. *Biophys. J.* 76:2502–2519.

van Workum, M., S. J. M. van Dooren, N. Oldenburg, D. Molenaar, P. R. Jensen, J. L. Snoep, and H. V. Westerhoff. 1996. DNA supercoiling depends on the phosphorylation potential in *Escherichia coli*. *Mol. Microbiol.* 20:351–360.

White, J. H. 1969. Self-linking and the Gauss integral in higher dimensions. *Am. J. Math.* 91:693–728.

Zakharova, S. S., W. Jesse, C. Backendorf, S. U. Egelhaaf, A. Lapp, and J. R. C. van der Maarel. 2002. Dimensions of Plectonemically Supercoiled DNA. *Biophys. J.* 83:1106–1118.